CHAPTER - VII

Structure and Dielectric Behaviour of Co-doped Barium Titanate Nanoparticles

Chapter-VII

Structure and Dielectric Behaviour of Co-doped Barium Titanate Nanoparticles

7.1. Introduction

Barium titanate ($BaTiO_3$, BT) has become increasingly important in the electro-ceramic industry, because of its ferroelectric, piezoelectric and thermoelectric properties [1]. Also it has been widely studied due to its important applications in nonlinear optics [2-4], multilayer ceramic capacitors (MLCC), transducers, actuators and ferroelectric random access memories (FRAM) [5,6] etc. Bulk BT has ABO_3 (Ba^{2+} as A and Ti^{4+} as B) perovskite structure. Above the Curie temperature T_C ~ 130 ^oC [7], it has a centro-symmetric cubic crystal (c) structure (P_{m3m} space) with A at the corners, B at the center, and the O^{2-} at the face centers. Kwei et al [8] reported that as the temperature is lowered, it passes through three different polymorphic phases such as tetragonal of P_{4mm}, orthorhombic (o-phase I) of A_{mm2} and rhombohedral of R_{3m} space group. The phases arise due to elongation of the cubic lattice along an edge (001), a face diagonal (011) and along a body diagonal (111) respectively. Among these structures, the orthorhombic structure is rather complex due to the large uncertainty of its structural parameters [9,10].

With the miniaturization of electronic devices, it is scientifically interesting and technologically challenging to synthesize and characterize ultrafine barium titanate powders. In BT nanocrystals, the structural and physical properties are strongly dependent on the grain size. With decreasing grain size, an anomalous lattice expansion and decrease in tetragonality were experimentally observed at room temperature [11]. It was demonstrated that, with decreasing grain size, the lattice constant 'a' of BT nanoparticles increased anomalously in both the tetragonal and the cubic phases, while the lattice constant 'c' decreased, which resulted in a decrease in tetragonality [12]. Nanocrystalline BT showed that with decreasing size, the cubic-tetragonal transition temperature shifts downward while the tetragonal-orthorhombic transition temperature shifts upward before getting suppressed [12]. Although it is believed that the crystal structure plays a crucial role in ferroelectric properties, few systematic studies are available on the crystal structure of nanoparticles [9,13].

The dopants have a significant effect on the structural and dielectric properties of bulk BT. It is known that a high dielectric constant and good temperature stability in BT can be achieved through addition of dopant. It is reported that the TiO_6 octahedra are disturbed with B-site doping resulting broadening of the transition at T_C [14]. Specifically doping with 3d transition elements in BT stabilizes a different structural configuration in the system [15]. It is possible to tailor the parameters such as maximum dielectric constant (ε_m), transition temperature T_C, and $\frac{d\varepsilon}{dT}$ by a suitable doping. In our previous work [16] we showed that dielectric permittivity in Fe^{3+} doped specimens is enhanced compared to that of undoped BT ceramics and T_C shifted to lower value with increasing dopant concentration. The enhancement of dielectric permittivity was explained in terms of the change in crystalline structure. Quite similar results were shown by doping with nickel ion [17]. Doping with MgO, it was seen that the orthorhombic phase exists even at room temperature [18]. Jiang et al [19] observed multiple-twins and intergrowth structures containing a $P6_3/mmc$ hexagonal (h) phase in small BT particles. The c-BT with traces of h-phase occurs in D ~ 20 nm [20]. Quite similar to this, we reported [21] a new polymorph of P_{nma} orthorhombic structure (o-phase II) forms at temperature as small as 450-550 ^oC. As analyzed with X-ray diffraction, when heating at temperature as high as 650 ^oC, it converts in part to the t-phase in a strictly controlled way of thermal induced intergrowth, resulting in a hybrid composite.

Doped BT in many cases have superior and stable property than pure BT. But all the facts are only verified for micron sized BT particles. To our knowledge there is no report on structural and dielectric properties of transition metal doped BT nanoparticles. Owing to these points, it is important to examine structure and stability in doped BT small particles in order to filling-up the gap in our basic understanding of the phase diagram, ferroelectricity, and other properties.

We report structural and dielectric properties of Co ion doped BT nanoparticles. A polymer template of Ba^{2+}, Ti^{4+}, Co^{2+}, and polyvinyl alcohol (PVA) has been used to obtain such crystallites. After annealing at 750 ^0C for 2h, the x-ray diffraction analysis showed the $BaTi_{1-x}Co_xO_3$ is a hybrid composite polymorph of o-BT-II and tetragonal BT. Doping with Co^{2+} ions support the o-BT-II favorably to coexist as a majority phase in a hybrid composite structure. Dielectric properties also support the polymorphic change with doping.

7.2. Experimental Procedure

7.2.1. Sol-gel Synthesis

Cobalt doped BT, with compositions $Ba(Ti_{1-x}Co_x)O_3$ where, x = 0.03, 0.06, & 0.16, were prepared by a modified sol-gel route. The polymer template in Ba^{2+} and Ti^{4+}/Co^{2+} cations arranged via PVA molecules was obtained by dispersing barium acetate, tetra-isopropyl orthotitanate ($C_{12}H_{28}O_4Ti$) and cobalt nitrate [$Co(NO)_3$,$6H_2O$] in PVA as explained in the next section.

First of all, a solution of ethyl alcohol and acetic acid in the volume ratio of 3:1 was prepared. Weighted amount of tetraisopropyl orthotitanate was hydrolyzed in that solution and the mixture (A) were stirred for 2h. Dispersed Ba^{2+} ion through aqueous barium acetate (1.07M) was poured into the solution (A) and the resulting mixture (B) was stirred for another 1h. The solution B was clear and transparent. In the next stage the Co^{2+} through aqueous cobalt nitrate (0.043 to 0.343 M) was added to the precursor B. Finally aqueous PVA (3.0 g/dl) was added drop-wise to this solution in a ratio of 5:2. The polymer precursor can very efficiently adjust the size of the grain [22]. Depending on the PVA molecular structure in a dispersive medium, Ba^{2+}, Ti^{4+} and Co^{2+} cations can be dispersed and arranged via PVA in a number of ways. The aqueous sample of 3 g/dl PVA in this experiment provides a huge amount of active OH^- groups. Such OH^- groups act as head groups in PVA to attract and absorb the Ba^{2+}, Ti^{4+} and Co^{2+} cations over the molecular PVA surfaces in a specific template structure as reported in the case of synthesizing a similar precursor for lead zirconate titanate or CrO_2 nanoceramics [19,20]. Thus the polymer serves as a surfactant to encapsulate the cationic species in divided groups during the reaction. A controlled reaction occurs that confine the size and morphology of the specimen. In PVA there are several processes of hydrolysis and poly-condensation involve, resulting in a polymer gel at room temperature. The gel was dried (in oven 70 ^oC for 24h) calcined at 750 ^oC to crystallize the BT phase.

7.2.2. Characterization

The crystal structure was investigated using powder X-ray diffractometer (Model PW1710, CuK_α radiation, $2\theta=3^o$-130^o, $\Delta 2\theta=0.03^o$). The average grain diameter of the crystallites (D) were calculated from X-ray diffraction peaks widths β (= $\Delta 2\theta_{1/2}$) using Debye – Scherrer relation

$$D = \frac{0.9\lambda}{\beta \cos\theta}$$

Where λ is the wavelength and θ is the angle of diffraction.

The microstructure of the specimens was observed under Transmission Electron Microscope (TEM, Philips, Model-CM12). The nano-grains were chemically analyzed with Energy Dispersive Absorption (EDAX) spectra. For investigation under TEM the powder samples were dispersed in an acetone medium by ultrasonic vibrator. The dispersed samples were placed drop-wise on a carbon coated Cu grid. After drying for a few hours these grids were placed inside the TEM. The calcined powders were isostatically pressed into pellets under pressure of 5 bars for 5 minutes. The pellets were sintered at 1000 ^{o}C for 2h for the measurement of dielectric permittivity. The capacitance of the sample was measured by using a LCR meter (Agilent-4284A) in the range of temperature from 30 ^{o}C to 200 ^{o}C.

7.3. Results and Discussion

7.3.1. X-ray diffraction and microstructure

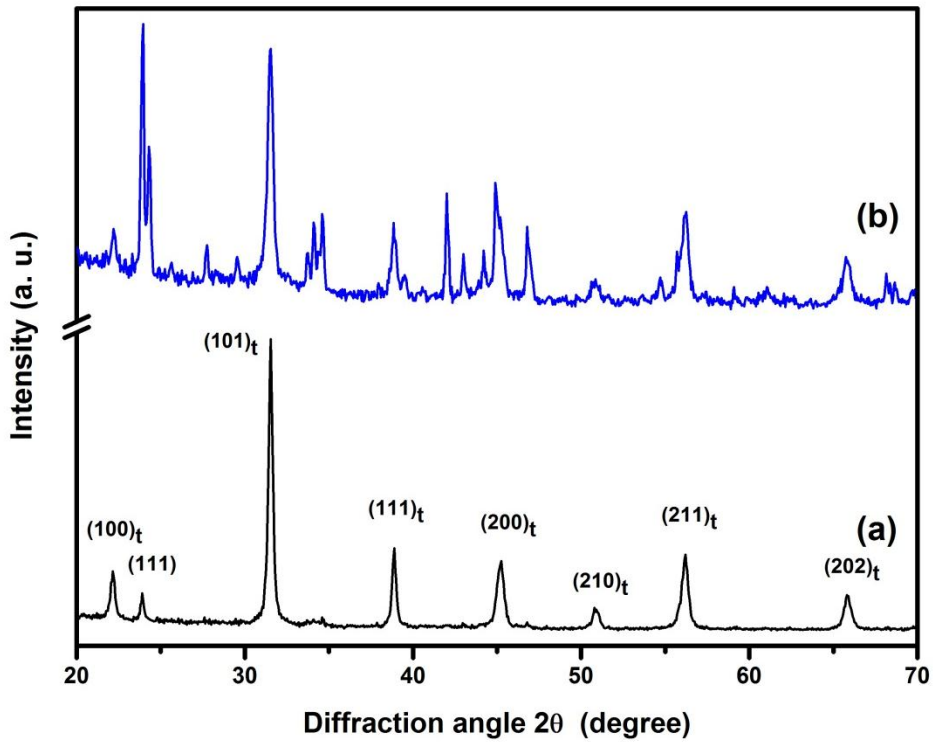

Figure 7.1 *X-ray diffraction patterns showing controlled t- BT to o- BT phase transformation in a nano composite structure after doping with (b)1.6 mole % Co ion, comparing with (a) Undoped BT.*

Figure 7.1 shows the XRD patterns of BT specimen doped with 1.6 mole % of cobalt ions, derived after heating a polymer precursor at 750 ^{0}C for 2h in air. Figure

7.1(a), patterns from undoped BT specimen, compares with the diffractograms obtained from doped specimens. The pattern consists of 8 – 27 distinct peaks between 20^0 and 70^0 on the 2θ scale with relative peak intensities $I_P \geq 5$. The variations in peak intensities I_P and interplanar spacings d_{hkl} reveal that a new series of peaks associated with a new orthorhombic structure have been developed in sample doped with different mole % of cobalt ions in addition to tetragonal phase.

Table 7.1 *Observed d_{hkl} values in t-BT and o-BT polymorphs in a nanocomposite structure.*

d_{hkl}(nm)		I_p	h k l	
Observed	Calculated		o-BT	t-BT
0.3992	0.3992	18		1 0 0
0.3692	0.3692	11	1 1 1	
0.2839	0.2838	100		1 0 1
0.2311	0.2313	27		1 1 1
0.2004	0.1996	22		2 0 0
0.1793	0.1785	6		2 1 0
0.1634	0.1633	25		2 1 1
0.1419	0.1419	10		2 0 2

The calculated d_{hkl} values refer to a = 0.6393 nm, b = 0.5268 nm, c = 0.8824 nm in o-BT while a = 0.3992 nm and c = 0.4035 nm in t-BT. The sample was heated at 750 ℃ for 2h.

The diffractogram in Figure 7.1 (a) has a total of eight distinct peaks in the specified range of pure BT. This is a simple diffractogram similar to a report in a P_{4mm} tetragonal (t) phase [23] but the d_{hkl} values do not fit well with the d values having a = 0.3994 nm & c = 0.4036 nm [23(d)]. The diffractogram in Figure 7.1 (a) is characteristically the tetragonal BT polymorph with modified a = 0.3992 nm & c = 0.4035 nm with an extra peak at d_{hkl} = 0.3692 nm which is vividly discussed in our previous article [21]. We showed that the extra peak accompanied with more peaks exist at lower annealing temperature indicating the formation of new o-BT-II phase of space group P_{nma} with average lattice parameters a = 0.6393 nm, b = 0.5268 nm and c = 0.8824 nm. This o-BT-II crystal yields unit cell lattice volume V = 0.2971 nm^3 or density 5.214 g cm^{-3}, assuming z = 4 BT formula units. With the increase of annealing temperature this phase transformed into tetragonal phase of a = 0.3992 nm and c = 0.4035 nm. Thus the extra peak in Figure 7.1(a) is originating due to the (111) reflection of new orthorhombic crystal structure (o-BT-II). Thermodynamically, it is a metastable phase of a high volume

or Gibbs free energy. The o-BT-I (A_{mm2} space group) has 14 distinct diffraction peaks of this region with a = 0.3987 nm, b = 0.5675 nm, c = 0.5690 nm, V = 0.1287 nm^3 (z = 2) and ρ = 6.018 $g.cm^{-3}$ [23(c)]. In Table 7.1 all the observed diffraction peaks in Figure 7.1 (a) are indexed in terms of d_{hkl} values in representative (hkl) reflections, with a standard deviation ± 0.0005 nm, assuming both tetragonal and new o-BT-II phase. The tetragonal phase exist as large a fraction as 91 vol % (determined by I_p values in the peaks in the two phases) with the o-BT-II phase in this nanocomposite structure.

Table 7.2 *Assignments of observed d_{hkl} values in t-BT and o-BT polymorphs in a 0.6 mole % Co doped BT structure.*

d_{hkl}(nm)		I_p	h k l	
Observed	Calculated		o-BT	t-BT
0.3995	0.3997	12		1 0 0
0.3720	0.3719	100	1 1 1	
0.3655	0.3649	52	1 0 2	
0.3208	0.3206	14	2 0 0	
0.3009	0.3015	5	2 0 1	
0.2842	0.2842	55		1 0 1
0.2646	0.2662	8	0 2 0	
0.2623	0.2624	25	2 1 1	
0.2569	0.2599	28	2 0 2	
0.2365	0.2370	5	1 2 1	
0.2315	0.2316	19		1 1 1
0.2274	0.2283	10	0 2 2	
0.2147	0.2151	36	1 2 2	
0.2090	0.2097	17	1 0 4	
0.2043	0.2048	21	2 2 0	
0.2019	0.2020	41		0 0 2
0.1996	0.1998	18		2 0 0
0.1937	0.1951	28	1 1 4	
0.1785	0.1787	5		2 1 0
0.1675	0.1704	10	0 2 4	
0.1646	0.1667	14	3 2 0	
0.1633	0.1635	23		2 1 1
0.1558	0.1560	7	3 2 2	
0.1419	0.1421	10		2 0 2
0.1375	0.1386	14	0 3 4	
0.1364	0.1373	9	4 2 0	

The calculated d_{hkl} values refer to a = 0.6412 nm, b = 0.5325 nm, c = 0.8875 nm in o-BT while a = 0.3997 nm and c = 0.4041 nm in t-BT. The sample has been heated at 750 ℃ for 2h.

After doping with Co ions both t- and o-BT-II phases were modified largely. The diffractograms of sample doping with different mole % of Co have a total of 27 distinct

peaks in the 20-70^0 range of the diffraction angle 2θ. For the doped specimens the observed diffraction peaks are indexed in terms of d_{hkl} values in representative (hkl) reflections. A set of observed and calculated d_{hkl} values in 0.6 mole % Co ion doped BT is given in Table 7.2.

Table 7.3 *The average values of particle size (D), lattice volume V, lattice number z and density ρ in both the phases of o- BT(II) and t- BT in nanocomposite structure.*

Sample	o-BT (II)				t- BT (z =1)		
	D (nm)	V (nm^3)	z	ρ (g/cm^3)	D (nm)	V (nm^3)	ρ (g/cm^3)
Undoped BT	29	0.2971	4	5.214	28	0.06430	6.023
0.3 mole% Co^{2+}-BT	25	0.2975	4	5.207	26	0.06445	6.009
0.6 mole% Co^{2+}-BT	21	0.3030	4	5.112	19	0.06456	5.999
1.6 mole% Co^{2+}-BT	23	0.3007	4	5.151	23	0.06451	6.004
Bulk BT	--	0.1287	2	6.018	--	0.06440	6.016

The values for the bulk crystals are reported from literature [23]. The bulk o- BT has a different space group A_{mm2} than the nanocrystals of a P_{nma} space group.

Table 7.4 *The lattice parameters, surface areas S_0, and volume fraction (φ) of o- BT(II) phase after heating a polymer template at 750 ^{0}C for 2 h in air.*

Specimens	Lattice parameters (nm)			S_0 (nm^2)	S_0/V_0 (nm^{-1})	φ
	a	b	c			
Undoped BT	0.6393	0.5268	0.8824	2.7314	9.1935	9
0.3 mole% Co^{2+}-BT	0.6395	0.5271	0.8825	2.7334	9.1879	38
0.6 mole% Co^{2+}-BT	0.6412	0.5325	0.8875	2.7662	9.1294	64
1.6 mole% Co^{2+}-BT	0.6405	0.5297	0.8865	2.7534	9.1566	52
Bulk BT	0.3987	0.5675	0.5690	1.5518	12.0574	--

The φ value is reported for the o-BT-II phase.

It is noted that in this Co doped BT specimen, the lattice parameters of o-BT-II crystal structure is modified with a = 0.6412 nm, b = 0.5325 nm and c = 0.8875 nm and the tetragonal structure is changed with lattice parameter of a = 0.3997 and c = 0.4041. Similar changes in lattice parameter are observed in other doped specimens.

The crystallite sizes, lattice volumes, and densities of the specimens are compared in Table 7.3. The lattice parameters, surface areas S_0, volume fraction of o-

BT-II phase are depicted in Table 7.4. These data are obtained after a thorough analysis of the XRD patterns.

In the specimens, the lattice volumes of o-BT-II phases are approximately double the volume of bulk BT (o-BT-I). Volume fraction of o-BT-II is large for the samples with larger lattice volume. The largest volume fraction of o-BT-II phase is 64 vol % for 0.6 mole % Co ion doped BT. Large lattice expansions have been observed in BT nanoparticles [16,24,25]. Computer simulation on BT clusters show that the origin of lattice expansion is due to the increase in ionicity because different bond lengths elongate and subsequently Ba-O bonds expand [15].

In our previous work [21], BT nanoparticles were synthesized using polymer molecule of polyvinyl alcohol. The polymer burnt off upon heating in air at temperature as high as 450 ^{0}C, resulting in a P_{nma} orthorhombic crystal structure (o-BT-II). As large a fraction as ~55 vol % was promoted to t-BT at temperature as high as 650 ^{0}C. Raising the temperature further to 750 ^{0}C, the fraction became 72 %. Like other parameters it is also noted from Table 7.4 that, S_0 = 2.7662 nm^2 which is the largest at 0.6 mole % Co ion doped BT. The large lattice volume is associated with excess surface area of the nanocrystallites. Thermodynamically, these are metastable phases of a high volume or Gibbs free energy which supports the BT to occur and exist in that specific polymorph. In this case a kinetically different reaction process is operating in small BT reaction species by doping with transition metal ion like Co in the environment of polymer precursor. Under controlled conditions of the nucleation and growth, as in this example of a PVA polymer template, the S_0 value provides an important process parameter to initiate and drive growth of BT with a high value of the Gibb's free energy.

To compute an average D value, specimens were measured very precisely by scanning the selected XRD peaks at a high resolution. Broader peaks due to a small D value of the sample in this example are not affected by the instrumental broadening, i.e. an order of a lower value. Usually a strain broadening imparts a small fwhm value and that is neglected here in computing the average D value. D = 29 nm value is determined with the fwhm values from the diffraction peaks of pure BT. To confirm the particle size of nano BT, the samples were investigated through bright field image by the Transmission Electron Microscope. A typical micrograph from specimens 0.6 mole % Co ion doped BT is shown in Figure 7.2 (a). Average particle diameter was calculated from the micrographs. The results extracted from TEM reasonably agree with these

obtained from XRD. Selected area diffraction patterns were taken from the specimens. A typical pattern from specimens 0.6 mole % Co ion doped BT is shown in Figure 7.2 (b). The d values calculated from these figures support the values calculated from XRD data. Thus, it is seen that the polymer precursor in the specimens can very efficiently adjust the size of the grains. The PVA molecules absorb Ba^{2+}, Ti^{4+} and Co^{2+} cations over the molecular PVA surfaces in a specific template structure. Despite the organic counterpart disintegrates a refined template species is retained in local structures. A reaction rate limited growth of Ba^{2+}, Ti^{4+}, Co^{2+} and O^{2-} thus occurs in divided groups of small templates. To investigate the chemical composition of the specimens, EDAX by High Resolution Transmission Electron Microscope was carried out. The matrix of the EDAX show strong Ba, Ti, O, and Co peaks. No trace of carbonate is evident.

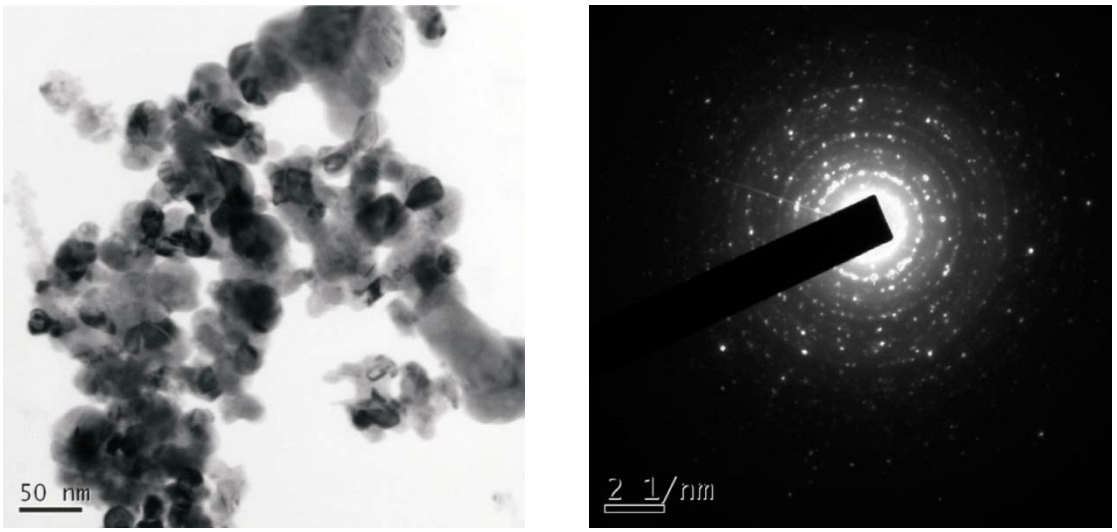

(a) **(b)**

Figure 7.2 *(a) Bright field Transmission Electron Micrographs of 0.6 mole % Co ion doped BT nanocrystals and (b) Selected Area Diffraction patterns of 0.6 mole % Co ion doped BT nanopowders.*

The effect of Co ion doping on the growth of o-BT-II phase in BT nanocrystal is further evidenced by a close up view of the diffractogram in Figure 7.3. The peaks $(100)_t$, (111) and (102) shift to larger 2θ values creating possible ionic vacancies or other defects [26-28]. The donor/acceptor ratio is known to have significant effect on the microstructure of BT ceramics. Because of the existence of two cation sites in the perovskite, a foreign ion can occupy either the Ba^{2+} site or the Ti^{2+} site depending on its ionic radius and charge. The transition metal ions preferably substitute the Ti^{4+} sites. It was earlier reported that Ni ion acted as electron acceptor in BT lattice [17]. Here, the

size of Co^{2+} ions (0.78Å) matches with the size of Ti^{4+} ion (0.68 Å). But due to larger size of Co^{2+} ions an expansion of lattice volume is expected which is experimentally evident from XRD results as summarized in Table 7.3.

The incorporation of Co^{2+} ions is compensated with the formation of oxygen vacancies to maintain electro neutrality as shown below:

$$CoO + Ti_{Ti} + O_O \rightarrow Co''_{Ti} + V_O^{\cdot\cdot} + TiO_2$$

Kroger-Vink notation is used in the above equation to describe the defect species. Microstrain is developed in the system due to creation of vacancies [26-28]. The defects have also important contribution on dielectric property of the specimens as explained later. As a result of doping there exist significant values of microstrains as well as macrostrains, which support so-called a high-energy self-stabilized composite structure to form and exist up-to some doping.

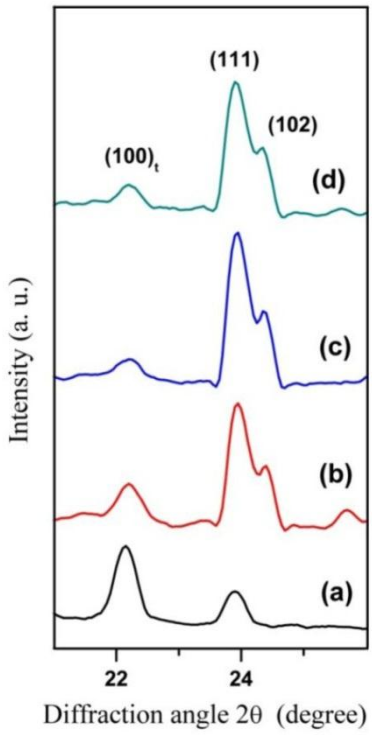

Figure 7.3 *A close-up of view of the XRD patterns in the range $2\theta = 21^0$ - 26^0 showing shifts in $(100)_t$, (111) and (102) peaks of o- BT specimens with (b) 0.3 mole % Co ion (c) 0.6 mole % Co ion and (d) 1.6 Co mole % Co ion, comparing with (a) Undoped BT after heating at 750 ^{0}C for 2 h in air.*

Technologically, this is a useful physical parameter to design and fabricate mechanically toughened ceramics and products by kind of a mechanism of the internal

transformation-toughness similar to that well-established in stabilized zirconia and derived components of high-energy metastable ceramics [29,30].

7.3.2. Dielectric Properties

The dielectric properties of the specimens were measured at different frequencies ranging from 1 kHz to 1 MHz varying the temperature from room temperature to 200 ^{0}C. After measuring the capacitance C, ε_r value has been obtained with $\varepsilon_r = \frac{C\,t}{\varepsilon_0 A}$ where ε_0 is the permittivity of vacuum space, *t* the sample thickness (2.5–3 mm), and *A* the area (~43 mm^2) of a top electrode. In Figure 7.4, dielectric constants of the specimens versus temperature at 10 kHz frequency are plotted. The measurement of dielectric constant was done both in heating and cooling cycle. No significant hysteresis was observed.

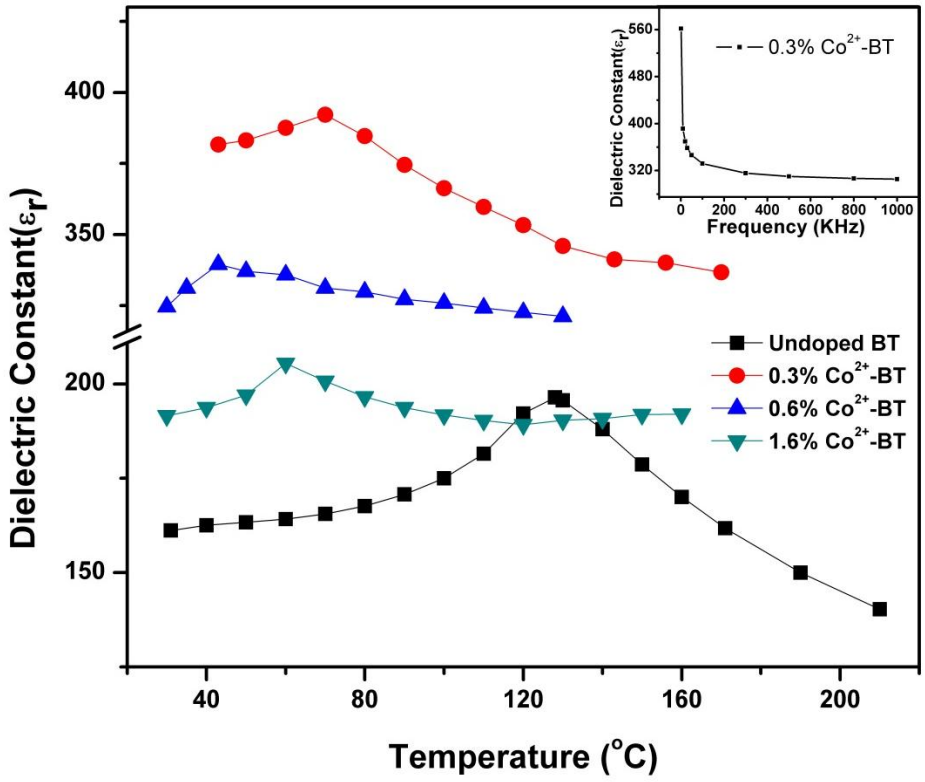

Figure 7.4 *Variation of dielectric constants with temperature obtained at a signal frequency of 10 kHz.*

It is seen that the doped specimens possess higher dielectric constant compared to undoped BT. In the inset of Figure 7.4, the variation of permittivity with frequency in the range from 100 Hz to 1 MHz is shown. This indicates the presence of space charge characteristics in this system. The effect of space charge polarization decreases with the

increase of the signal frequency. Figure 7.5 shows the variation of tanδ (dielectric losses) with temperature from the specimens at a signal frequency of 10 kHz. It is seen that the dielectric losses remain always less than 1, but the losses in the doped specimens are higher than the undoped samples. As explained in the previous section, the incorporation of Co^{2+} ions is compensated by the formation of oxygen vacancy defects. These defects result an enhanced dielectric constant and dielectric loss by the way of space charge polarization. The dielectric permittivity data was also fitted with the Curie-Weiss law $\frac{1}{\varepsilon} = \frac{T-T_0}{C}$. It is seen that the dielectric data deviates largely from the law in case of the doped specimens. It was earlier established that the dielectric constant of a system containing nanoparticles should have different values as the grain boundary of the nanoparticles contain a large density of defects [31,32]. These defects can cause a space charge distribution in interfaces. Thus the grain boundaries in nanostructured Co-doped have an important effect on its dielectric property.

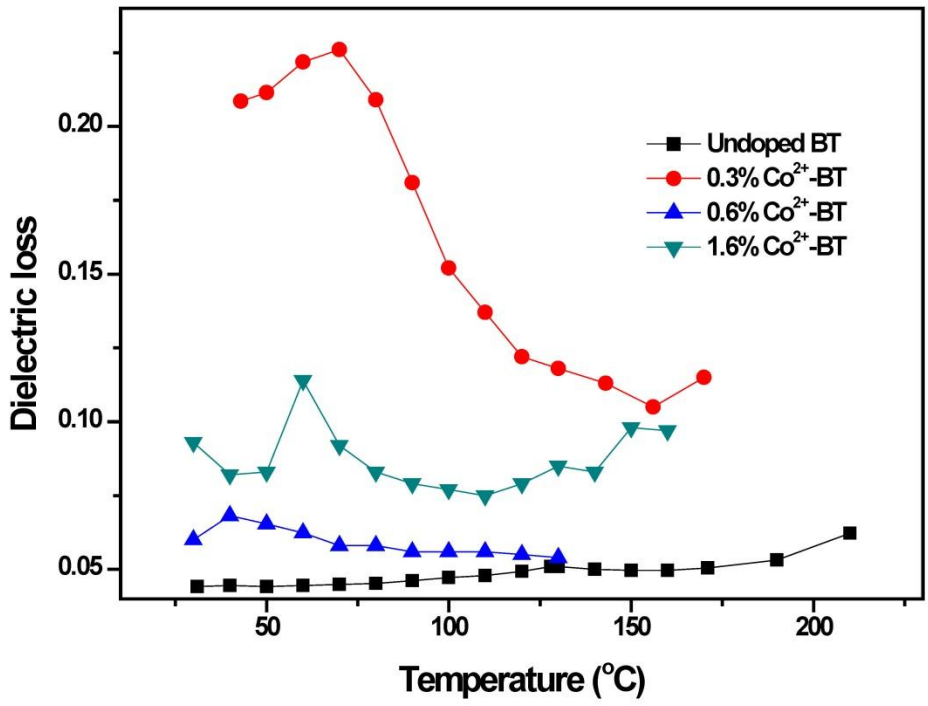

Figure 7.5 *Variation of dielectric loss with temperature obtained from the specimens at 10 kHz signal frequency.*

Here, the room temperature dielectric permittivity of the specimens at 10 kHz frequency lies in the ranges from 160 to 375 substantially lower than the values of BT in μm size but quite close to the values of BT nanoparticles as reported earlier. Few reports show that room temperature dielectric constant of 0.3–0.5 μm sized BT ceramics was

equal to 2000 when measured at 10 kHz [18,33,34]. Similarly few reports [35,36] show that ε_r = 230 and 700 for 25 nm and 40 nm grain sized specimens. Dielectric constants of the present set of specimens are lower than the values of containing micron-sized crystallites but close to the values of BT nanoparticles. In doped specimens, dielectric constant decreases gradually with the increase of doping concentration as shown in Figure 7.5. Initial enhancement of dielectric constant after doping was attributed to space charge polarization. The doped specimens are nanocomposite systems containing both orthorhombic and tetragonal BT phases. With the increase of dopant concentration the volume fraction of o-BT-II phase increases and shows the maximum (of 64 vol %) in 0.6 mole % Co-doped specimen. The mixing rule would be applied to explain the result if the relative dielectric permittivity of two phases were known. Also the grain boundaries in nanostructured Co-doped have an important effect on its dielectric property. There should have a solubility limit of Co- ions in nano BT as the transition metal ions are soluble to a maximum of 2 mole % in micron sized BT [16,37]. The excess Co ions (if any) modify the space charge polarization at the grain boundaries and reduce the dielectric constant. Thus at this moment we are not able to state a specific reason for the decrease of dielectric property with the increase of dopant concentration. Electrical conductivity of the composites will be helpful for making the picture clearer. The broadening in ε_r–T curve at transition temperature reveals that the specimens have a diffuse transition. A broad peak in the temperature dependence of dielectric permittivity is the feature of ferroelectrics with a diffuse phase transition. Here, the broadening means the widening of fwhm of ε_r–T curve. The present broadening in the T_C transition is partly due to strain generated by defects similar to Hennings et al. work. It was also reported [38-40] that the broadening in the T_C transition occurs due the inhomogeneous distribution of the stress and electric field.

Undoped BT shows the ferroelectric – paraelectric transition (T_C) at 128 ^oC. T_C strongly depends upon the doping concentration in the specimen. In doped specimens, T_C decreases gradually with the increase of doping and it shows a minimum value of 43 ^oC for 0.6 mole % Co ion doped specimen. The dependence of T_C on the concentration of doping in micrometer sized BT was reported [41,42]. Dielectric behavior in those cases were explained in terms of the change in crystalline structure of doped BT specimen. Also it is reported [14] that with the increase of doping content (Zr ion), the tetragonal to orthorhombic phase transition moves to higher temperatures, whereas the tetragonal to

cubic phase transition moves down to reduced temperature. It was found that at certain percentage of doping orthorhombic – tetragonal and tetragonal – cubic transition temperature coalesce and above the critical percentage of doping, the tetragonal and orthorhombic phases disappear and the ferroelectric rhombohedral phase changes directly into the paraelectric cubic phase. The average particle sizes in these specimens were in the range of 1 to 50 μm. In our work the doped BT nanoparticles are under stress due to presence of a secondary phase as discussed in previous section. As a result the individual orthorhombic – tetragonal and tetragonal – cubic transition did not occur and the two transitions coalesce giving single broad transition peak. Doping with Co^{2+} ion on BT changes the volume fraction of o-BT-II phase or tetragonal phase and this change is reflected to dielectric properties. Here the variation of T_C with doping is someway related to the variation of φ value as shown in Table 7.4, i.e. higher the content of o-BT-II phase lowers the T_C. The stabilization of the lower symmetry phases by Co^{2+} ion doping is similar to the case of "pinching" upon the Ti-site substitution. The phase coexistence has been discussed in connection with the diffuse nature of the phase transformation of the solid solutions. In the Co^{2+} doped BT system, with the Co^{2+} ions substituting Ti^{4+} ions of BT, a larger distortion of the lattice may take place with the generation of oxygen vacancies. So, in this case, the local random electrical field and strain field will be strong, which could contribute to a more pronounced abnormal dielectric behavior and a larger shifting of T_c.

7.4. Conclusions

We have synthesized Co^{2+} ion doped BT nanoparticles through a modified sol-gel route using PVA as capping agent. The concentration of the dopant varies from 0.3 mole % to 1.6 mole %. The average crystallite size ranges from 21 nm – 29 nm. The PVA molecules adsorb Ba^{2+}, Ti^{4+} and Co^{2+} cations over the molecular PVA surfaces in a specific template structure. Despite the organic counterpart disintegrates a refined template species retain in local structures. A reaction rate limited growth of Ba^{2+}, Ti^{4+}, Co^{2+} and O^{2-} thus occurs in divided groups of small templates. The XRD analysis indicates that a new P_{nma} orthorhombic (o-BT-II) structure with average lattice parameters a = 0.6393 nm, b = 0.5268 nm and c = 0.8824 nm exist in the specimens. The lattice volume V = 0.2971 nm^3 of o-BT-II with z = 4 formula units, yields a density ρ =

5.214 gm/c.c. With the doping of Co ion the volume fraction of o-BT-II phase increases. In 0.6 mole % Co doped specimen o-BT-II exist with 64 vol % volume fraction.

Doped BT possesses higher values of permittivity than undoped specimens. Room temperature dielectric constant increases from a value of 160 to 375. The presence of space charge polarization in the system is the reason behind the enhancement of dielectric properties. The ferroelectric – paraelectric transition temperature decreases from 128 ^{0}C to a minimum value of 43 ^{0}C for the specimens doped with 0.6 mole % dopant. The coexistence of tetragonal and orthorhombic phase has been discussed in connection with the diffuse nature of the dielectric behavior. The presence of secondary phase o-BT-II, have an important role in controlling the dielectric properties of the specimens.

7.5. References

[1] P. P. Phule and S. H. Risbud, *J. Mater. Sci.* **25**, 1169 (1990).

[2] W. Y. Shih, W. H. Shih, and I. A. Aksay, *Phys. Rev. B* **50**, 15575 (1994).

[3] Y. Luo, I. Szafraniak, N. D. Zakharov, V. Nagarajan, M. Steinharf, R. B. Wehrspohn, J.H. Wendorff, R. Ramesh, and M. Alexe, *Appl. Phys. Lett.* **83**, 440 (2003).

[4] H. Fu and L. Bellaiche, *Phys. Rev. Lett.* **91**, 257601 (2003).

[5] S. Mathews, R. Ramesh, T. Venkateasan, J. Benedetto, *Science* **276**, 238 (1997).

[6] B. H. Park, B. S. Kang, S. D. Bu, T. W. Noh, J. Lee, W. Jo, *Nature* **401**, 682 (1999).

[7] B. Jaffe, W. R. Cook, and H. Jaffe, *Piezoelectric Ceramics*, Academic Press, London, U.K., 1971.

[8] G. H. Kwei, A. C. Lawson, S. J. L. Billinge and S. W. Cheong, *J. Phys. Chem.* **97**, 2368 (1993).

[9] G. Arlt, D. Hennings, and G. de. With, *J. Appl. Phys*. **58**, 1619 (1985).

[10] E. K. Akdogan, M. P. Leonard and A. Safari, "*Size effects in ferroelectric ceramics*" in Handbook of Low and High Dielectric Constant Materials for Applications, Vol. 2, Edited by H. S. Nalwa. Academic Press, 1999.

[11] B. D. Begg, E. R. Vance, and J. Nowotny, *J. Am. Ceram. Soc*. **77**, 3186 (1994).

[12] M. H. Frey and D. A. Payne, *Phys. Rev. B* **54**, 3158 (1996).

[13] R. Asiaie, W. Zhu, S. A. Akbar and P. K. Dutta, *Chem. Mater*. **8**, 226 (1996).

[14] D. Hennings, A. Schnell, and G. Simon, *J. Am. Ceram. Soc*. **65**, 539 (1982).

[15] H. T. Langhammer, T. Muller, K. H. Felgner, and H. P. Abicht, *J. Am. Ceram. Soc*. **83**, 605 (2000).

[16] A. Jana, T. K. Kundu, S. K. Pradhan and D. Chakravorty, *J. Appl. Phys*. **97**, 044311 (2005).

[17] A. Jana and T. K. Kundu, *Mater. Lett*. **61**, 1544 (2007).

[18] T. Nagai, K. Iijima, H. J. Hwang, M. Sando, T. Sekino and K. Niihara, *J. Am. Ceram. Soc*. **83**, 107 (2000).

[19] B. Jiang, J. L. Peng, L. A. Brusill, T. L. Ren, P. L. Zhang, and W. L. Zhong, *Physica B* **291**, 203 (2000).

[20] W. S. Cho, *J. Phys. Chem. Solids* **59**, 659 (1998).

[21] A. Jana, S. Ram, T. K. Kundu, *Philos. Mag*. **87**, 5485 (2007).

[22] T. T. Fang, H. L. Hseih and F. S. Shiau, *J. Am. Ceram. Soc*. **76**, 1205 (1993).

[23] X-ray powder diffraction files (Joint Committee on Powder Diffraction Standards, Swarthmore, Pennsylvania: International Centre for Diffraction Data, 1999), (a) 41-0373 (o-$BaCO_3$), (b) 79-2263 (c-$BaTiO_3$), (c) 81-2200 (o-$BaTiO_3$), (d) 81-2204 (t-$BaTiO_3$), (e) 82-1175 (h- $BaTiO_3$), and (f) 85-1798 (r- $BaTiO_3$).

[24] K. Ishikawa and T. Uemori, *Phys. Rev*. **60**, 11841 (1999).

[25] R. A. Young and D. B. Wiles, *J. Appl. Crystallogr*. **15**, 430 (1982).

[26] S. S. Jida and T. Miki, *J. Appl. Phys*. **80**, 5234 (1996).

[27] L. Guo, S. Yang, C. Y. Yu, P. J. Wang, W. Ge and G. K. L. Wong, *Appl. Phys. Lett.* **76**, 2901 (2000).

[28] S. Ram and T. K. Kundu, *J. Nanosci. Nanotechnol*. **4**, 1076 (2004).

[29] Z. Jing, C. Ang, Z. Yu, P. M. Vilarinho, and J. L. Bapista, *J. Appl. Phys*. **84**, 983 (1998).

[30] A. H. Heuer, N. Claussen, W. M. Kriven and M. Ruhle, *J. Am. Ceram. Soc*. **65**, 642 (1982).

[31] H. Gleiter, *Prog. Mater. Sci*. **33**, 223 (1989).

[32] W. P. Halperin, *Rev. Mod. Phys*. **58**, 533 (1986).

[33] X. Wang, M. Gu, B. Yang, S. Zhu and W. Cao, *Microelectron. Eng*. **66**, 855 (2003).

[34] M. P. McNeal, S. J. Jang, and R. E. Newnham, *J. Appl. Phys*. **83**, 3288 (1998).

[35] M. H. Frey, D. A. Payne, *Appl. Phys. Lett*. **63**, 2753 (1993).

[36] M. B. Park, N. H. Cho, C. D. Kim and S. K. Lee, *J. Am. Ceram. Soc*. **87**, 510 (2004).

[37] M. T. Buscaglia, V. Buscaglia, M. Viviani, P. Nanni, M. Hanuskova, *J. Eur. Ceram. Soc.* **20**, 1997 (2000).

[38] J. C. Cheng, J. Tang, X. J. Meng, S. L. Guo, J. H. Chu, A. M. Wang, H. Wang, and Z. Wang, *J. Am. Ceram. Soc*. **84**, 887 (2001).

[39] H. Shimooka and M. Kuwabara, *J. Am. Ceram. Soc.* **78**, 2849 (1995).

[40] P. Pinceloup, C. Courtois, A. Leriche, and B. Thierry, *J. Am. Ceram. Soc*. **82**, 3049 (1999).

[41] D. D. Fong, G. B. Stephenson, S. K. Streiffer, J. A. Eastman, O. Auciello, P. H. Fuoss and C. Thomson, *Science* **304**, 1650 (2004).

[42] Z. Jing, Z. Yu and C. Ang, *J. Mater. Sci.* **38**, 1057 (2003).